Journal of Quantitative Spectroscopy & Radiative Transfer 112 (2011) 457–464

Contents lists available at ScienceDirect

Journal of Quantitative Spectroscopy & Radiative Transfer

journal homepage: www.elsevier.com/locate/jqsrt

Mid-infrared absorption cross sections for acetone (propanone)

Jeremy J. Harrison [a,*], Neil Humpage [b], Nicholas D.C. Allen [a], Alison M. Waterfall [c], Peter F. Bernath [a], John J. Remedios [b]

[a] Department of Chemistry, University of York, Heslington, York YO10 5DD, United Kingdom
[b] Earth Observation Science, Department of Physics & Astronomy, University of Leicester, University Road, Leicester LE1 7RH, United Kingdom
[c] Rutherford Appleton Laboratory, Science and Technology Facilities Council, Didcot OX11 0QX, United Kingdom

ARTICLE INFO

Article history:
Received 16 July 2010
Received in revised form
2 September 2010
Accepted 3 September 2010

Keywords:
Acetone
Propanone
High-resolution Fourier transform spectroscopy
Infrared absorption cross sections
Remote sensing
Atmospheric chemistry

ABSTRACT

Infrared absorption cross sections for acetone (propanone) have been determined in the 830–1950 cm^{-1} spectral region from spectra recorded using a high-resolution FTIR spectrometer (Bruker IFS 125HR) and a multipass cell with a maximum optical path length of 19.3 m. The spectra of mixtures of acetone with dry synthetic air were recorded at 0.015 cm^{-1} resolution (calculated as 0.9/MOPD using the Bruker definition of resolution) at a number of temperatures between 194 and 251 K and pressures appropriate for atmospheric conditions. Intensities were calibrated using three acetone spectra (recorded at 278, 293 and 323 K) taken from the Pacific Northwest National Laboratory (PNNL) IR database. The new absorption cross sections have been combined with previous high spectral resolution results to create a more complete set of acetone absorption cross sections appropriate for atmospheric remote sensing. These cross sections will provide an accurate basis for upper tropospheric/lower stratospheric retrievals of acetone in the mid-infrared spectral region from ACE and MIPAS satellite data.

1. Introduction

Acetone (C_3H_6O), also known as propanone, is the simplest member of the ketone family, and one of the most abundant volatile organic compounds (VOC) within the free troposphere with a background concentration of up to 0.5 ppb in clean air at northern mid-latitudes [1,2]. Acetone has an important influence on the oxidising capacity of the atmosphere and indirectly on cloud nucleation and the production of low level ozone [3–5]. However, despite the significant importance of acetone's chemistry in the atmosphere, the acetone budget is poorly constrained [5]. This is partly due to the localised nature of some of the sources and sinks of acetone.

Acetone production is cyclical with maximum emissions in the Northern Hemisphere observed in late spring and summer, with a minimum in the winter [6]. Background concentrations of acetone in the Southern Hemisphere are somewhat lower, whereas the largest emissions in the tropics are observed in the dry season [7]. Acetone is also a tropospheric tracer with a short lifetime estimated to be between two and four weeks [8–10].

Acetone has a large biogenic source, including plant growth and decay [11,12]. The most significant contributor to the atmospheric loading of acetone is the oxidation of organic precursors, also emitted from biogenic sources, including alkanes, alkenes and terpenes [8,13–15]. The reaction of propane with hydroxyl (OH) radicals is thought to contribute considerably to the secondary production of acetone with up to 80% of propane following this reaction pathway and forming about 16–21 Tg yr^{-1} of acetone [8,16]. Highly elevated acetone concentrations have been observed in biomass burning plumes which are another important source [17,18]. Anthropogenic sources, including

* Corresponding author. Tel.: +44 1904 434589; fax: +44 1904 432516.
E-mail address: jjh506@york.ac.uk (J.J. Harrison).

0022-4073/$ - see front matter © 2010 Elsevier Ltd. All rights reserved.
doi:10.1016/j.jqsrt.2010.09.002

motor vehicle and industrial emissions, are estimated to have a smaller contribution to the acetone budget [19].

Sinks for acetone include the reaction with hydroxyl radicals [20] and photolysis in the troposphere [21,22], in which the molecule dissociates into acetyl (CH_3CO) and methyl (CH_3) radicals. The acetyl radical in the free troposphere is a major source of peroxyacetyl nitrate (PAN) [23]. The lifetime of PAN, which acts as a carrier for reactive NO_x ($NO+NO_2$), increases from a few hours at the Earth's surface to several months at the tropopause, due to its greater thermal stability at lower temperatures. The relatively long lifetime in the middle and upper troposphere allows it to be transported over long distances, translating to a long-distance transport of NO_x. PAN catalyses the formation of ozone [16,24], which is mostly produced from the photolysis of NO_2. Therefore acetone has an indirect effect on the production of tropospheric ozone, which is a potent greenhouse gas and is also toxic [2].

The predominant source of HO_x in the troposphere is through the reaction of $O(^1D)$ with H_2O [3,25]. In the drier upper troposphere photolysis of acetone is the dominant source of OH [20]. Increasing the oxidising capacity of the upper troposphere accelerates the conversion of NO_x into HNO_3 and HNO_4, and to a lesser extent sulphur containing compounds are also oxidised to form H_2SO_4 [26]. The tropospheric production of sulphuric and nitric acids is important in the activation and nucleation of aerosols [3,23]. Despite the reduction in NO_x, due to oxidation, PAN production is driven by the increased formation of HO_2 caused by acetone photolysis.

There has been significant disagreement as to the importance of the photolysis sink for acetone. Initial work on the photodissociation quantum yields of acetone in the UV region showed that the rate was pressure- and temperature-dependent, and predicted that photolysis of acetone was the main sink mechanism [27]. However, Arnold et al. [10] used the chemical transport model TOMCAT and new acetone quantum yields to show that the photolysis sink was far smaller than had previously been thought and that attack by OH was the main sink mechanism for acetone.

A recent study [28,29] has suggested that acetone uptake by the ocean may be as large as 62 Tg yr^{-1}, making this the largest sink. However, other studies have concluded that acetone is emitted from the ocean [30], particularly by aerobic marine bacteria [31,32]. Dry and wet deposition are minor sinks for acetone [8,33].

The first atmospheric measurements of acetone were published by Cavanagh et al. in 1969 [34]. Clean Arctic air was sampled using gas chromatography and the results showed a significant and fairly stable background concentration of acetone with an average value of 0.8 ppb. The first measurements above the boundary layer were taken by aircraft up to an altitude of 6 km [24], giving a mean acetone concentration of 1.14 ppb. More recent ground-based measurements and aircraft campaigns have determined acetone concentrations in the upper troposphere—lower stratosphere (UTLS) from Arctic, [35] tropical [12,33] and mid-latitude background air [36], as well as from biomass burning plumes [18,33]. Little data has been obtained in the Southern Hemisphere, and due to the regionality of acetone sources it is difficult to estimate the overall global budget from individual measurements. Previous budget estimates for the annual global emissions of acetone have ranged from about 40 to 95 Tg [8–10]. The use of remote-sensing techniques allows greater global coverage, although so far there have been no global measurements of acetone. Remedios et al. [37] first demonstrated that acetone could be retrieved remotely from thermal emission spectra using the MIPAS-B2 instrument. Acetone was detected using the band at 1218 cm^{-1}, with a volume mixing ratio of 0.53 ppb obtained at 10 km.

Increasingly satellite instruments are able to directly observe VOCs in the atmosphere. In particular, the Atmospheric Chemistry Experiment (ACE), on board SCISAT-1, is able to detect more organic molecules in the troposphere than any other satellite instrument. In fact, the first detection of acetone using satellite infrared occultation spectroscopy was made by the ACE-FTS instrument, which sampled a biomass burning plume near the east coast of Tanzania on 8 October 2005 [38]. ACE uses a high-resolution Fourier transform spectrometer that covers the spectral region from 750 to 4400 cm^{-1} [39]. Due to this extended spectral coverage, it is possible to carry out retrievals in the strong 3 μm region, where all aliphatic hydrocarbons have their strongest-intensity modes (C–H stretch) and where there are relatively few spectral interferers.

Retrievals of concentration profiles from satellite data require accurate laboratory spectroscopic measurements in the form of either line parameters or absorption cross sections. The HITRAN database [40] is a good source of such spectroscopic data; however, it does not contain acetone. Acetone data are also contained in the Pacific Northwest National Laboratory (PNNL) IR database (http://nwir.pnl.gov/) [41], however these are not suitable for remote sensing of the UTLS for a number of reasons. All PNNL spectra are recorded at relatively low resolution (0.112 cm^{-1}) as mixtures with pure nitrogen gas, not synthetic air, at pressures of 760 Torr and temperatures of 278, 293 or 323 K.

The sparsity of good spectroscopic acetone data for remote sensing purposes can be explained by the experimental difficulties involved in taking the measurements. Acetone has a low vapour pressure ($\sim$1 Torr at 213 K and $\sim$0.2 Torr at 197 K) [42], meaning that long optical pathlengths must be used for spectroscopic measurements in order to achieve sufficient signal to noise ratios. Until now the most suitable dataset available for remote sensing of the UTLS in the midwave infrared (MWIR) region is that by Waterfall [43,44]. This is based on a number of pure and air-broadened acetone spectra recorded between 700 and 1780 cm^{-1} spectral region at 0.030 cm^{-1} resolution for the temperatures 224, 233, 253, 272 and 297 K. The aim of the present work was to extend the Waterfall dataset to lower temperatures, and to verify the consistency between measurements by repeating a small number for comparison.

Infrared absorption cross sections in the 3 μm region for acetone [45] have recently been determined. In a similar manner, high-resolution (0.015 cm^{-1}) spectra of

acetone/synthetic air have been recorded over a range of pressures and temperatures (50–370 Torr and 194–251 K), and used to derive infrared absorption cross sections for air-broadened acetone in the MWIR region between 830 and 1950 cm^{-1}. When used for remote sensing, it is important that the spectra are recorded at a high enough resolution, determined by the Doppler or pressure broadening, to resolve all the molecular features. This prevents errors creeping into the retrieval when the forward model is convolved with the instrumental lineshape (ILS) function of the FTS instrument.

This MWIR region covers three main vibrational band systems for acetone. The first of these is associated with a C–C stretch (ν_{17} with a frequency of 1216 cm^{-1}), and the third with a C=O stretch (ν_3; 1731 cm^{-1}). The second band has major contributions from CH_3 symmetrical deformation modes (ν_5 and ν_{16}; 1364 cm^{-1}), and weaker contributions from CH_3 "degenerate" deformation modes (ν_4, ν_{15} and ν_{21}, 1435, 1410 and 1454 cm^{-1} respectively) [46].

2. Experimental

Experiments were performed at the Molecular Spectroscopy Facility (MSF) located at the Rutherford Appleton Laboratory (RAL), Oxfordshire, UK. The measured air-broadened acetone absorption spectra were recorded using a Bruker Optics IFS 125HR high-resolution Fourier transform spectrometer (FTS) with a potassium bromide beamsplitter, mercury cadmium telluride (MCT) detector, and an internal mid-infrared radiation source (globar). An optical filter restricted the throughput to the spectral region below 2000 cm^{-1} and above the detector cut-off at 690 cm^{-1}. The aperture diameter (2.5 mm) of the spectrometer was set so that the intensity of infrared radiation falling on the MCT detector was maximised without saturation or loss of spectral resolution. All spectra were recorded at a resolution of 0.015 cm^{-1} (calculated as 0.9/MOPD using the Bruker definition of resolution). Norton–Beer weak apodisation and Mertz phase corrections were applied to all interferograms. The FTS was evacuated to a pressure below 0.2 Pa by a turbomolecular pump to minimise the absorbance of impurity atmospheric gases in the optical path. The FTS instrumental parameters and settings are summarised in Table 1.

A more detailed description of the experimental setup can be found in Ref. [45]. All measurements utilised the MSF short-path absorption cell (SPAC) [47]. The SPAC is a multipass cell with mirrors at each end to reflect the radiation back and forth across the length of the cell multiple times. These mirrors are fully adjustable from outside the cell, allowing the optical pathlength to be altered from 1.7 to 19.3 m in steps of 1.6 m. Transfer-optics are used to transfer the radiation from the spectrometer into the cell, and from the cell onto the external MCT detector.

The SPAC can be operated from room temperature down to 77 K, although the measurements in this work only go as low as 194 K. The temperature can be automatically controlled for extended periods of time. The actual cell temperature is monitored by six platinum resistance thermometers (PRT) situated at positions throughout the cell. The pressure in the cell is measured by three Baratron capacitance manometers (full scale 1, 10 and 1000 Torr).

Table 1
FTS and SPAC configurations.

Source	Globar
Detector	Mercury cadmium telluride
Beam splitter	Potassium bromide
Resolution	0.015 cm^{-1}
Aperture size	2.5 mm
Optical filter	177 (Northumbria Optical Coatings Ltd.)
Apodisation function	Norton–Beer Weak
Phase correction	Mertz
Cell windows	Potassium bromide
Transfer-optics chamber windows	Potassium bromide
Mirror coatings	Gold
Pressure gauges	3 MKS-690 A Baratrons (1, 10 and 1000 Torr)
Thermometry	6 PRTs, Labfacility IEC 751 Class A

Sample mixtures were prepared by introducing a small amount of cold acetone vapour directly into the cell and then adding dry synthetic air. Acetone (Merck Uvasol, $\geq$ 99.9% purity) was purified to remove dissolved air using multiple freeze-pump-thaw cycles. Dry synthetic air ('Air Zero Plus', Air Products, 20.9% $O_2 \pm 0.2\%$, $H_2O \leq 0.5$ ppm, $CH_4 \leq 0.05$ ppm, $CO+CO_2 \leq 0.1$ ppm, 99.99990% overall purity) was used 'as is' without additional purification. Details of the pressures, temperatures, SPAC optical pathlengths and the number of scans taken for each sample are contained in Table 2. Scans of pure N_2O were also recorded for the purposes of frequency calibration. Additionally, evacuated-cell background scans were recorded before and after the scan blocks for each sample. Ideally, an equivalent number of background scans as sample scans were measured to ensure sufficient signal to noise ratios when calculating transmittance spectra. The spectral baseline decreased by several percent throughout the course of a day, hence using averages of backgrounds recorded before and after, these drifts had little effect on the final cross sections.

The temperatures and pressures of the samples in the SPAC were logged every few seconds. The variations in these quantities were used to estimate their experimental uncertainties, which are given in Table 2. Overall the recorded temperatures showed good stability to within $\pm 0.5\%$ of the tabulated value.

The tabulated acetone partial pressures at the lowest temperatures are somewhat unreliable because they reflect the initial pressure before the addition of synthetic air. This addition resulted in a small increase in the temperature, which in turn increased slightly the acetone partial pressure. This has made it necessary to normalise the measurements against an accurate intensity standard. In this work we have chosen to use acetone spectra from the PNNL IR database. This is discussed further in Section 3.

The error in the SPAC optical pathlengths (see Table 2) at room temperature is estimated to be $\pm 0.2\%$. The pathlength

Table 2
Summary of the sample conditions for all scans in this work.

Acetone pressure (Torr)	Total pressure (Torr)	Temperature (K)	Pathlength (m)[a]	No. of scans[b]
0.020	50.2 ± 0.3	194.3 ± 1.0	17.71	300
0.041	49.8 ± 0.3	197.8 ± 1.0	17.71	200
0.041	74.9 ± 0.7	197.2 ± 1.0	17.71	300
0.041	99.4 ± 1.0	196.8 ± 1.0	17.71	300
0.100	75.7 ± 0.5	214.5 ± 0.7	6.51	300
0.100	148.7 ± 1.2	213.9 ± 0.8	6.51	280
0.093	74.6 ± 0.4	224.0 ± 0.7	6.51	300
0.093	149.3 ± 0.9	223.5 ± 0.8	6.51	300
0.622	162.4 ± 0.3	251.2 ± 0.4	1.71	300
0.615	370.2 ± 0.5	250.7 ± 0.4	1.71	300

[a] Error in the optical pathlength is estimated to be $\pm 0.2\%$ at room temperature.
[b] Note that each sample requires the measurement of a similar number of background scans taken with the same spectrometer settings. One scan takes about 33 s.

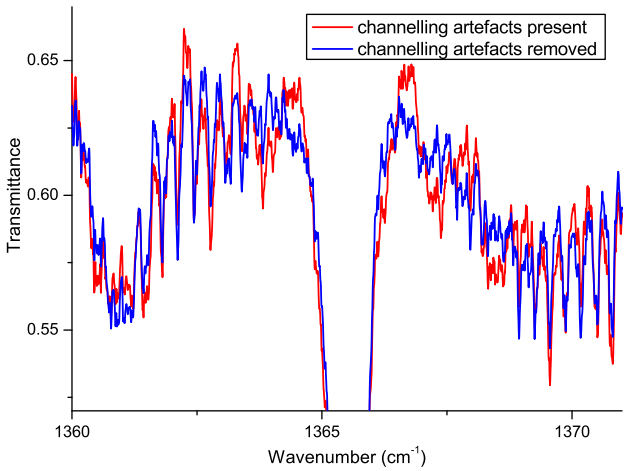

Fig. 1. A transmission spectrum recorded at 194.3 K and 50.2 Torr, which has had all the 'ghost' peaks responsible for channel fringes directly removed from the interferogram, compared with the resulting spectrum once all the channelling has been satisfactorily removed using the method described in the text. Residual channelling artefacts in the first case are clearly observed around the strong acetone Q branch.

changes slightly as the cell is cooled because the mirrors and optical components change position as they contract in size. Any systematic error in the pathlength will be accounted for by normalising against acetone spectra from the PNNL IR database.

The photometric uncertainty is estimated to be 2%, and the overall uncertainties in the absorption cross sections reported in this work are estimated to be 4%.

3. Results and discussion

Due to the non-linear response of MCT detectors to the detected radiation, which results in baseline perturbations, all interferograms were re-transformed using the non-linearity correction in Bruker's OPUS software.

Channel fringes were present in all the recorded spectra. Multiple reflections from optical components such as cell or transfer-optics windows have the effect of introducing weaker centreburst 'echoes' into the interferogram, which appear in the spectrum as sinusoidal modulations. These were observed during previous 3 μm acetone measurements [45], where they were simply removed by dividing sample scans by background scans. However, in the case of the present measurements the frequency components of the oscillations varied slightly from scan to scan, so simple division was not an option.

In general channelling can be minimised by removing the appropriate 'ghost' peaks in the interferogram, however this can sometimes introduce artefacts into the spectrum. This technique was successful for removing the fringes from background scans, and for the weakest channelling components of sample scans, however removing the strongest component from each sample scan required more effort. Fig. 1 gives a comparison of a transmission spectrum recorded at 194.3 K and 50.2 Torr, which has had all the 'ghost' peaks (including the one corresponding to the strongest component) directly removed from the interferogram, with the resulting spectrum once all the channelling has been satisfactorily removed. Residual channelling artefacts for the former are clearly observed around the strong acetone Q branch. In

the end, this channelling was removed by stretching and shifting the periodic oscillations of the corresponding strongest channelling component from a background scan until they matched those from a sample scan as closely as possible. Simple division removed essentially all of the channelling, although in a few cases weak residual oscillations (of the order of 0.1%) remained.

Transmission spectra were calculated by dividing averaged single-channel sample scans by appropriate averaged single-channel background scans. A further small correction was necessary to ensure that the baseline extended to 100% transmittance outside the absorption band. Spectral frequencies were calibrated using pure N_2O spectra, which were recorded during the experimental run. The accurate positions of isolated N_2O absorption lines between 1140 and 1320 cm^{-1} were determined from the HITRAN database [40].

Although care was taken to prevent impurities entering the cell by using high purity gases and pumping out the gas line before the preparation of sample mixtures, absorption lines of water were observed in the sample scans. Most of these lines were located in the region 1400–1700 cm^{-1}, between the main acetone bands, and were removed by hand.

Due to the temperature sensitivity of the acetone vapour pressure at low temperatures, the amount of absorber in the SPAC optical pathlength was relatively uncertain. For this reason, the *y*-axis of the cross sections derived in this work were calibrated using acetone spectra from the PNNL IR database. Each PNNL spectrum is a composite of multiple pathlength–concentration burdens, and great care has been taken to ensure that sample concentrations have been determined accurately. The accuracy of spectra in the PNNL database is quoted as 2.1% [41]. This calibration also relies on the fact that band intensities for isolated bands comprising primarily fundamentals are essentially independent of temperature [45,48,49]. Wang et al. [50] have previously determined integrated band strengths of acetone in the region of 830–3200 cm^{-1} at 233, 260 and 295 K, observing a moderate increase in band intensity with decrease in temperature (see Table 3). For the three principal bands recorded in this work, they observed increases in approximately 7% between 295 and 233 K. This temperature dependence is not supported by the PNNL spectra (at 278, 293 and 323 K), the spectra recorded in this work (214 K and above), nor the spectra recorded by Waterfall [43,44].

Additional acetone scans were measured over the 1000–4000 cm^{-1} spectral range at room temperature and 760 Torr of added synthetic air in order to check the relative intensities of the three MWIR bands with the previously measured 3 μm band [45]. It is particularly important to ensure that the spectroscopy is consistent between these two regions. The measurements confirmed that the relative intensities were consistent with spectra in the PNNL database within 0.5%.

Spectral absorption cross sections, $\sigma(\upsilon,P_{air},T)$, with units cm^2 $molecule^{-1}$, were calculated by the equation

$$\sigma(\upsilon,P_{air},T) = -\xi\frac{10^4 k_B T}{Pl}\ln\tau(\upsilon,P_{air},T) \quad (1)$$

where $\tau(\upsilon,P_{air},T)$ is the transmittance at wavenumber υ (cm^{-1}), temperature T (K) and synthetic air pressure P_{air}, P is the pressure of the absorbing gas (Pa), l the optical pathlength (m), k_B the Boltzmann constant ($=1.3806504\times10^{-23}$ $J\,K^{-1}$) and ξ the averaged factor required to satisfy the two normalisation requirements:

$$\int_{1025\ cm^{-1}}^{1930\ cm^{-1}}\sigma(\upsilon,P_{air},T) = 5.451\times10^{-17}\ cm\,molecule^{-1}(\pm0.1\%) \quad (2)$$

$$\int_{1152\ cm^{-1}}^{1631\ cm^{-1}}\sigma(\upsilon,P_{air},T) = 2.958\times10^{-17}\ cm\,molecule^{-1}(\pm0.1\%) \quad (3)$$

The values on the right hand side of Eqs. (2) and (3) are the average integrated band strengths of the three acetone PNNL spectra (recorded at 278, 293 and 323 K) in the ranges 1025–1930 cm^{-1} and 1152–1631 cm^{-1}, respectively, converted from PNNL units using the factor $k_B\times296\times\ln10\times10^4/0.101325$. Following this normalisation, the cross sections were re-baselined if required to ensure agreement with the PNNL baselines, and then normalised again. The final cross sections have typical signal to noise ratios (RMS) ranging from 300 to 500.

Table 3 provides a comparison of integrated band strengths for the three main acetone bands, averaged over all the absorption cross sections determined in this work. The wavenumber regions are the same as those of Wang et al. [50] for comparison purposes. Since the acetone bands overlap slightly, caution must be taken when making comparisons in this way. The integrations in Eqs. (2) and (3) are taken over wavenumber limits where the baseline is as close to zero as possible.

A selection of acetone absorption cross sections is given in Figs. 2 and 3. In the first figure is a plot over the entire recorded spectral range at 194.3 K and 50.2 Torr. In Fig. 3 is a section of the three cross sections at ~197–198 K and 49.8, 74.9 and 99.4 Torr, showing the pressure

Table 3
A comparison of averaged integrated band strengths determined from this work with those of Wang et al. [50] over three wavenumber regions. The units are 10^{-17} cm $molecule^{-1}$.

	Temperature (K)	1158–1285 cm^{-1} (ν_{17})	1285–1620 cm^{-1} (ν_5, ν_{16}, ν_4, ν_{15}, ν_{21})	1620–1920 cm^{-1} (ν_3)
This work	–	1.096 ± 0.044	1.858 ± 0.074	2.445 ± 0.098
Wang	233	1.120 ± 0.015	1.883 ± 0.020	2.441 ± 0.066
	260	1.082 ± 0.009	1.816 ± 0.013	2.358 ± 0.047
	295	1.041 ± 0.004	1.742 ± 0.009	2.266 ± 0.035

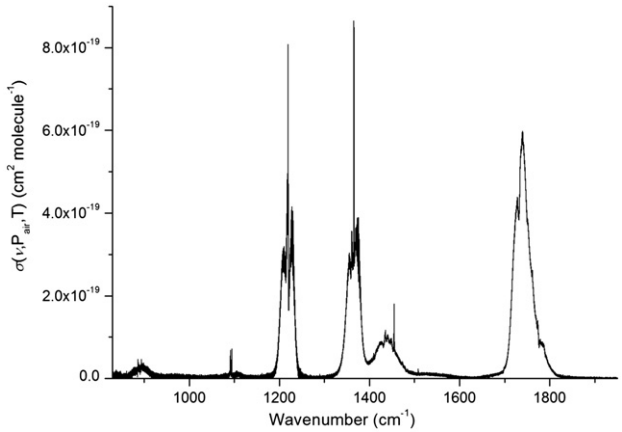

Fig. 2. Acetone absorption cross section at 194.3 K and 50.2 Torr.

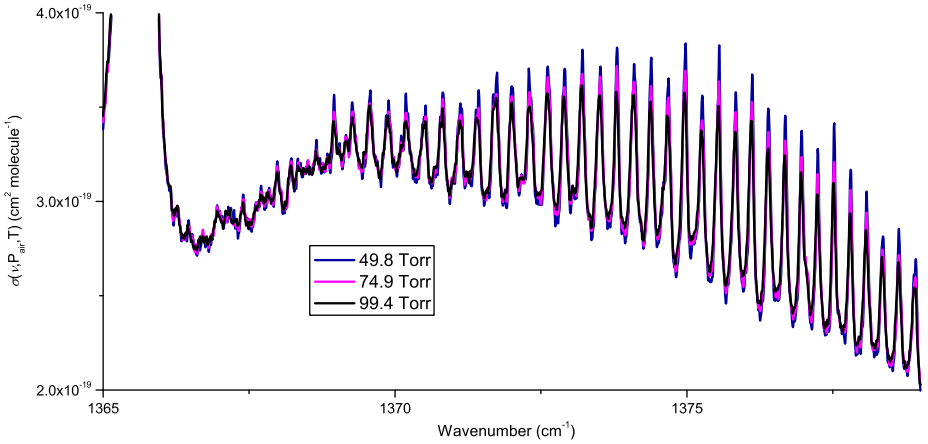

Fig. 3. Acetone absorption cross sections at ~197–198 K and 49.8, 74.9 and 99.4 Torr, showing the pressure dependence of the sharp structure near the *Q* branch at 1365 cm^{-1}.

dependence of the sharp structure near the *Q* branch at 1365 cm^{-1}.

The Waterfall measurements were recorded at the MSF using a Bruker Optics IFS 120HR FTS at a resolution of 0.030 cm^{-1} and aperture diameter of 1.7 mm, with a potassium bromide beamsplitter, MCT detector, and globar source. Norton–Beer strong apodisation and Mertz phase corrections were applied to the interferograms. It was observed that the low-pressure air-broadened Waterfall measurements are slightly under-resolved. For example, the cross section at 223.5 K and 149.3 Torr derived from this work, which closely matches the Waterfall cross section at 233.4 K and 149.9 Torr, indicates a difference of 2–3% in the fine structure. The higher pressure Waterfall cross sections are satisfactory due to the additional broadening of the structure.

The resolution can be defined as the full width at half maximum (FWHM) of the ILS of the FTS spectrometer, and depends on the apodisation function used. Bruker assumes a triangular apodisation function, defining resolution as 0.9/MOPD. The actual resolution of the Waterfall measurements (using Norton–Beer strong apodisation) is 0.966/MOPD [51,52], or 0.032 cm^{-1}, whereas for this work (using Norton–Beer weak apodisation) it is 0.724/MOPD [51,52], or 0.012 cm^{-1}. Furthermore, the pure acetone spectra of Waterfall should have been measured at a resolution slightly below the Doppler linewidth; for the ~1218 cm^{-1} acetone band at room temperature, this is about 0.002 cm^{-1}.

The most suitable set of acetone absorption cross sections for remote sensing of the UTLS region consists of

Table 4
Summary of the sample conditions for the Waterfall cross sections which have been combined into the final dataset.

Temperature (K)	Total pressure (Torr)
223.6	381.8
223.5	602.0
233.4	375.2
233.4	600.9
253.3	599.2
272.3	374.4
272.3	695.8
297.5	375.5
297.8	700.0

the cross sections determined in this work (corresponding to the conditions in Table 2), with a modified subset of the Waterfall ones (listed in Table 4). Errors for the Waterfall cross sections can be found in Refs. [43,44]. All pure and ~150 Torr cross sections have been discarded, as well as the one at 375.8 Torr and 253 K which has been replaced by the new measurement at 250.7 K and 370.2 Torr. The remaining Waterfall absorption cross sections have been re-normalised using Eq. (3) to agree with the PNNL database, which ensures that all cross sections in different spectral regions are consistent in intensity. This set of spectral absorption cross sections is available electronically upon request from the authors, and will be provided for inclusion in the HITRAN database.

4. Conclusions

High-resolution infrared absorption cross sections for acetone (between 830 and 1950 cm^{-1}) have been determined with an estimated uncertainty of 4%. Spectra were recorded for mixtures of acetone with dry synthetic air at 0.015 cm^{-1} resolution using a range of temperatures and pressures appropriate for atmospheric conditions and a multipass cell with a maximum optical pathlength of 19.3 m. Intensities were calibrated against three acetone spectra (recorded at 278, 293 and 323 K) taken from the PNNL IR database. A complete set of acetone absorption cross sections for remote sensing purposes has been created by combining these measurements with a modified and renormalized subset of the previous Waterfall measurements. These cross sections will provide an accurate basis for atmospheric retrievals of acetone in the mid-infrared spectral region from ACE [39] and MIPAS [53] satellite data.

Acknowledgements

The authors wish to thank the Natural Environment Research Council (NERC) for supporting J.J. Harrison through grant NE/F002041/1, and N.D.C. Allen through the National Centre for Earth Observation (NCEO), and for access to the Molecular Spectroscopy Facility (MSF) at the Rutherford Appleton Laboratory (RAL). R.G. Williams is thanked for providing technical support at the RAL.

References

[1] Chatfield RB, Gardner EP, Calvert JG. Sources and sinks of acetone in the troposphere—behaviour of reactive hydrocarbons and a stable product. J Geophys Res-Atmos 1987;92:4208–16.
[2] Singh HB, Kanakidou M, Crutzen PJ, Jacob DJ. High-concentrations and photochemical fate of oxygenated hydrocarbons in the global troposphere. Nature 1995;378:50–4.
[3] Folkins I, Chatfield R. Impact of acetone on ozone production and OH in the upper troposphere at high NO_x. J Geophys Res-Atmos 2000;105:11585–99.
[4] Wennberg PO, Hanisco TF, Jaegle L, Jacob DJ, Hintsa EJ, Lanzendorf EJ, et al. Hydrogen radicals, nitrogen radicals and the production of O_3 in the upper troposphere. Science 1998;279:49–53.
[5] Singh H, Chen Y, Staudt A, Jacob D, Blake D, Heikes B, et al. Evidence from the Pacific troposphere for large global sources of oxygenated organic compounds. Nature 2001;410:1078–81.
[6] Schade GW, Goldstein AH. Seasonal measurements of acetone and methanol: abundances and implications for atmospheric budgets. Global Biogeochem Cycle. 2006;20:10.
[7] Eerdekens G, Ganzeveld L, de Arellano JVG, Klupfel T, Sinha V, Yassaa N, et al. Flux estimates of isoprene, methanol and acetone from airborne PTR-MS measurements over the tropical rainforest during the GABRIEL 2005 campaign. Atmos Chem Phys 2009;9:4207–27.
[8] Singh HB, Ohara D, Herlth D, Sachse W, Blake DR, Bradshaw JD, et al. Acetone in the atmosphere—distribution, sources, and sinks. J Geophys Res-Atmos 1994;99:1805–19.
[9] Jacob DJ, Field BD, Jin EM, Bey I, Li QB, Logan JA, et al. Atmospheric budget of acetone. J Geophys Res-Atmos 2002;107:117.
[10] Arnold SR, Chipperfield MP, Blitz MA. A three-dimensional model study of the effect of new temperature-dependent quantum yields for acetone photolysis. J Geophys Res-Atmos 2005;110:114.
[11] Warneke C, Karl T, Judmaier H, Hansel A, Jordan A, Lindinger W, et al. Acetone, methanol, and other partially oxidized volatile organic emissions from dead plant matter by abiological processes: significance for atmospheric HO_x chemistry. Global Biogeochem Cycle 1999;13:9–17.
[12] Poschl U, Williams J, Hoor P, Fischer H, Crutzen PJ, Warneke C, et al. High acetone concentrations throughout the 0–12 km altitude range over the tropical rainforest in Surinam. J Atmos Chem 2001;38:115–32.
[13] Goldan PD, Kuster WC, Fehsenfeld FC. Nonmethane hydrocarbon measurements during the Tropospheric OH Photochemistry Experiment. J Geophys Res-Atmos 1997;102:6315–24.
[14] Orlando JJ, Noziere B, Tyndall GS, Orzechowska GE, Paulson SE, Rudich Y. Product studies of the OH- and ozone-initiated oxidation of some monoterpenes. J Geophys Res-Atmos 2000;105:11561–72.
[15] Reissell A, Harry C, Aschmann SM, Atkinson R, Arey J. Formation of acetone from the OH radical- and O_3-initiated reactions of a series of monoterpenes. J Geophys Res-Atmos 1999;104:13869–79.
[16] Singh HB, Hanst PL. Peroxyacetyl nitrate (PAN) in the unpolluted atmosphere – an important reservoir for nitrogen-oxides. Geophys Res Lett 1981;8:941–4.
[17] Holzinger R, Warneke C, Hansel A, Jordan A, Lindinger W, Scharffe DH, et al. Biomass burning as a source of formaldehyde, acetaldehyde, methanol, acetone, acetonitrile, and hydrogen cyanide. Geophys Res Lett 1999;26:1161–4.
[18] Yokelson RJ, Christian TJ, Karl TG, Guenther A. The tropical forest and fire emissions experiment: laboratory fire measurements and synthesis of campaign data. Atmos Chem Phys 2008;8:3509–27.
[19] Goldstein AH, Schade GW. Quantifying biogenic and anthropogenic contributions to acetone mixing ratios in a rural environment. Atmos Environ 2000;34:4997–5006.
[20] Jaegle L, Jacob DJ, Brune WH, Wennberg PO. Chemistry of HO_x radicals in the upper troposphere. Atmos Environ 2001;35:469–89.
[21] McKeen SA, Gierczak T, Burkholder JB, Wennberg PO, Hanisco TF, Keim ER, et al. The photochemistry of acetone in the upper troposphere: a source of odd-hydrogen radicals. Geophys Res Lett 1997;24:3177–80.
[22] Wollenhaupt M, Carl SA, Horowitz A, Crowley JN. Rate coefficients for reaction of OH with acetone between 202 and 395 K. J Phys Chem A 2000;104:2695–705.
[23] Arnold F, Burger V, DrosteFanke B, Grimm F, Krieger A, Schneider J, et al. Acetone in the upper troposphere and lower stratosphere: impact on trace gases and aerosols. Geophys Res Lett 1997;24:3017–20.
[24] Arnold F, Knop G, Ziereis H. Acetone measurements in the upper troposphere and stratosphere—implications for hydroxyl radical abundances. Nature 1986;321:505–7.
[25] Jaegle L, Jacob DJ, Wennberg PO, Spivakovsky CM, Hanisco TF, Lanzendorf EJ, et al. Observed OH and HO_2 in the upper troposphere suggest a major source from convective injection of peroxides. Geophys Res Lett 1997;24:3181–4.
[26] Arnold F, Schneider J, Gollinger K, Schlager H, Schulte P, Hagen DE, et al. Observation of upper tropospheric sulfur dioxide- and acetone-pollution: potential implications for hydroxyl radical and aerosol formation. Geophys Res Lett 1997;24:57–60.
[27] Gierczak T, Burkholder JB, Bauerle S, Ravishankara AR. Photochemistry of acetone under tropospheric conditions. Chem Phys 1998;231:229–44.
[28] Marandino CA, De Bruyn WJ, Miller SD, Prather MJ, Saltzman ES. Oceanic uptake and the global atmospheric acetone budget. Geophys Res Lett 2005;32:L15806, doi:10.1029/2005GL023285.
[29] Marandino CA, De Bruyn WJ, Miller SD, Prather MJ, Saltzman ES. Correction to "Oceanic uptake and the global atmospheric acetone budget. Geophys Res Lett 2006;33:L24801, doi:10.1029/2006GL028225.

[30] de Reus M, Fischer H, Arnold F, de Gouw J, Holzinger R, Warneke C, et al. On the relationship between acetone and carbon monoxide in different air masses. Atmos Chem Phys 2003;3:1709–23.
[31] Nemecek-Marshall M, Wojciechowski C, Kuzma J, Silver GM, Fall R. Marine vibrio species produce the volatile organic-compound acetone. Appl Environ Microbiol 1995;61:44–7.
[32] Nemecek-Marshall M, Wojciechowski C, Wagner WP, Fall R. Acetone formation in the vibrio family: a new pathway for bacterial leucine catabolism. J Bacteriol 1999;181:7493–9.
[33] Murphy J, Oram D, Reeves C. Measurements of volatile organic compounds over West Africa. Atmos Chem Phys Discuss 2010;10: 3861–92.
[34] Cavanagh LA, Schadt CF, Robinson E. Atmospheric hydrocarbon and carbon monoxide measurements at Point Barrow Alaska. Environ Sci Technol 1969;3:251–7.
[35] Solberg S, Dye C, Schmidbauer N, Herzog A, Gehrig R. Carbonyls and nonmethane hydrocarbons at rural European sites from the Mediterranean to the Arctic. J Atmos Chem 1996;25:33–66.
[36] Wohlfrom KH, Hauler T, Arnold F, Singh H. Acetone in the free troposphere and lower stratosphere: aircraft-based CIMS and GC measurements over the North Atlantic and a first comparison. Geophys Res Lett 1999;26:2849–52.
[37] Remedios JJ, Allen G, Waterfall AM, Oelhaf H, Kleinert A, Moore DP. Detection of organic compound signatures in infra-red, limb emission spectra observed by the MIPAS-B2 balloon instrument. Atmos Chem Phys 2007;7:1599–613.
[38] Coheur PF, Herbin H, Clerbaux C, Hurtmans D, Wespes C, Carleer M, et al. ACE-FTS observation of a young biomass burning plume: first reported measurements of C_2H_4, C_3H_6O, H_2CO and PAN by infrared occultation from space. Atmos Chem Phys 2007;7:5437–46.
[39] Bernath PF, McElroy CT, Abrams MC, Boone CD, Butler M, Camy-Peyret C, et al. Atmospheric chemistry experiment (ACE): mission overview. Geophys Res Lett 2005;32:L15S01, doi:10.1029/2005GL022386.
[40] Rothman LS, Gordon IE, Barbe A, Benner DC, Bernath PF, Birk M, et al. The HITRAN 2008 molecular spectroscopic database. JQSRT 2009;110:533–72.
[41] Sharpe SW, Johnson TJ, Sams RL, Chu PM, Rhoderick GC, Johnson PA. Gas-phase databases for quantitative infrared spectroscopy. Appl Spectrosc 2004;58:1452–61.
[42] Carl LYaws. In: Chemical properties handbook. McGraw-Hill; 1999.
[43] Waterfall AM. Measurement of organic compounds in the upper troposphere using infrared remote sensing. D.Phil. thesis, University of Oxford, 2004.
[44] Waterfall AM, Remedios JJ. Acetone infrared absorption cross sections for atmospheric remote sensing, in preparation.
[45] Harrison JJ, Allen NDC, Bernath PF. Infrared absorption cross sections for acetone (propanone) in the 3 μm region. J Quant Spectroscopy Radiat Transfer, in press, doi:10.1016/j.jqsrt.2010.08.011.
[46] Shimanouchi T. Molecular vibrational frequencies in NIST chemistry webbook, NIST standard reference database number 69, Eds. Linstrom PJ and Mallard WG, National Institute of Standards and Technology, Gaithersburg MD, 20899, http://webbook.nist.gov/.
[47] Paynter DJ, Ptashnik IV, Shine KP, Smith KM, McPheat R, Williams RG. Laboratory measurements of the water vapor continuum in the 1200–8000 cm^{-1} region between 293 and 351 K. J Geophys Res 2009;114:D21301, doi:10.1029/2008JD011355.
[48] Harrison JJ, Allen NDC, Bernath PF. Infrared absorption cross sections for ethane (C_2H_6) in the 3 μm region. J Quant Spectroscopy Radiat Transfer 2010;111:357–63, doi:10.1016/j.jqsrt.2009.09.010.
[49] Harrison JJ, Bernath PF. Infrared absorption cross sections for propane (C_3H_8) in the 3 μm region. J Quant. Spectroscopy Radiat Transfer 2010;111:1282–8, doi:10.1016/j.jqsrt.2009.11.027.
[50] Wang WF, Stevenson A, Reuter DC, Sirota JM. Absolute band intensities of acetone ($(CH_3)_2CO$) in the infrared region of 830–3200 cm^{-1} at low and room temperatures. Spectrochim Acta Part A 2001;57:1603–10.
[51] Norton RH, Beer R. New apodizing functions for Fourier spectrometry. J Opt Soc Am 1976;66:259–64.
[52] Norton RH, Beer R. Erratum to new apodizing functions for Fourier spectrometry. J Opt Soc Am 1977;67:419.
[53] Fischer H, Birk M, Blom C, Carli B, Carlotti M, von Clarmann T, et al. MIPAS: an instrument for atmospheric and climate research. Atmos Chem Phys 2008;8:2151–88.